Plasmonics (2022) 17:931–940
https://doi.org/10.1007/s11468-021-01579-3

Highly Sensitive Plasmonic Fiber-Optic Sensors using Group IV Transition Metal Nitrides: a Numerical Investigation

Yashar E. Monfared[1,2,3] · Barret L. Kurylyk[2] · Mita Dasog[1]

Received: 24 June 2021 / Accepted: 18 November 2021 / Published online: 13 January 2022
© The Author(s), under exclusive licence to Springer Science+Business Media, LLC, part of Springer Nature 2021

Abstract

We report a detailed theoretical and numerical investigation of the sensing mechanism and performance of plasmonic fiber-optic sensors using group IV transition metal nitrides. We first compared the plasmonic properties of hafnium nitride (HfN), zirconium nitride (ZrN), and titanium nitride (TiN) to gold (Au) as a conventional plasmonic material and designed two different plasmonic fiber-optic sensing platforms using side-polished single mode fibers and few mode fibers (FMFs). Using the finite element method, we demonstrated that the sensing mechanisms in the proposed sensors are based on the interplay between fiber and plasmonic modes and variation of resonance wavelength depending on analyte refractive index. We show that HfN and ZrN can considerably outperform Au in the visible region as alternative cost-effective plasmonic materials for the design of fiber-optic sensors with more than three times larger sensitivity and a sensing figure of merit of almost eight times that of Au. In particular, HfN-coated FMF sensors can demonstrate an average linear sensitivity of 6140 nm/RIU, a maximum sensitivity of 8200 nm/RIU, and an average (maximum) figure of merit of 133 (201) for analyte refractive indices between 1.33 and 1.38. We show that the figure of merit of the proposed simple side polished HfN coated FMF is more than four times larger than that of the previously reported similar fiber-optic sensors. The results show the potential of group IV transition metal nitrides, particularly HfN and ZrN, to replace Au in various fiber-optic applications including monitoring marine environments, medical diagnosis, and biosensing.

Keywords Fiber-optic sensor · Transition metal nitrides · Liquid analyte detection · Few mode fibers · Plasmonics

Introduction

Plasmonics is an emerging research area concerned with the nanoscale interaction of light and matter [1]. Oscillation of free electrons at a metal-dielectric interface stimulated by an incident electromagnetic radiation is called surface plasmon (SPs) [1]. When the frequencies of incident photons and SPs converge, maximum electron oscillation is achieved which is known as surface plasmon resonance (SPR) [1, 2]. As the resonance frequency strongly depends on the physical and chemical properties of the medium close to the material surface, the excitation of SPs provides an effective method to monitor the surrounding environment of a plasmonic nanostructure [2]. At resonance, a large portion of the incident light energy will transfer to surface electrons to excite SPs [2]. Therefore, one can expect to see a major dip (peak) in light transmission (absorption) spectra at resonance. By measuring the variations in transmission (or absorption) spectra of the incident light, which is related to energy consumption of SPs, the refractive index (RI) of an unknown analyte can be easily determined. This enables the structure to function as a sensor or biosensor [2, 3].

SPR sensing offers many advantages including high sensitivity, real-time measurements, and compatibility with existing optical devices like fiber optics [2, 3]. However, the bulky arrangement of the conventional prism-based SPR setups, for example, the Kretschmann configuration, is a major obstacle to the application of SPR sensors in biological and medical applications where small probe sizes are needed [3, 4]. Additionally, in some applications, for

✉ Yashar E. Monfared
y.monfared@dal.ca

[1] Department of Chemistry, Dalhousie University, 6274 Coburg Road, Halifax, Nova Scotia, Canada

[2] Center for Water Resources Studies and Department of Civil and Resources Engineering, Dalhousie University, Halifax, NS, Canada

[3] Lamont Doherty Earth Observatory, Earth Institute, Columbia University, Palisades, NY 10964, USA

example, environmental monitoring in ocean settings, it is often necessary to measure medium properties at distant and hard-to-reach locations in which prism-based SPR sensors cannot be used properly [4].

Fiber-optic based plasmonic sensors have the potential to overcome these challenges, while also offering new, transformative features such as immunity to electromagnetic interference, in situ measurements, capacity for distributed and quasi-distributed sensing, and the ability to simply integrate with other optical components [3–5]. These features potentially create novel opportunities for environmental monitoring applications. The sensing performance of plasmonic fiber-optic sensors is usually characterized by the sensitivity, the peak full width at half maximum (FWHM) to demonstrate the broadness of the peak, and the figure of merit (FOM) to relate the fiber sensitivity to its peak FWHM [6]. These parameters depend on the fiber geometry, fiber design parameters, and the plasmonic properties of the coating material [3, 6]. Various fiber types have been utilized in previous plasmonic fiber-optic studies including single-mode fibers (SMFs) [7], multi-mode fiber (MMFs) [8], photonic crystal fibers (PCFs) [5, 9], and few-mode fibers (FMFs) [6, 10].

Each fiber type has its own advantages and disadvantages. For instance, SMFs usually offer narrow peaks but suffer from the reduction of coupling efficiency between the light source and the fiber and are more sensitive to the polishing process and depth of the polished section [6]. MMFs have relatively large core diameters, which means high coupling efficiency with the light source and low sensitivity to the polishing process [6]. However, the large number (up to a few hundred) of propagating modes supported in the MMF will satisfy the phase matching condition between the core modes and the SP modes at various wavelengths [6]. As a result, the peak FWHM of the FMFs are usually broad, which reduces the sensor FOM. Conversely, PCFs can offer very high sensitivities and control over design parameters, but they suffer from complex fabrication processes and air hole deformations [3]. Reducing the number of modes using FMFs is one way to narrow the FWHM. Recent studies using FMFs for sensing applications have demonstrated a trade-off between MMF and SMFs in terms of coupling efficiency and peak FWHM [6, 10].

There have been several recent computational and experimental studies on the design of plasmonic fiber-optic sensors. For example, Coelho et al. [7] tested a plasmonic SMF sensor using gold (Au) and titanium dioxide (TiO_2) coating and reported a sensitivity up to 3800 and 5100 nm/RIU for the reflection and transmission modes. Dash and Jha [9] studied a plasmonic-based PCF sensor using graphene deposition on silver (Ag) and reported a sensitivity of up to 3700 nm/RIU. Jang et al. [10] studied a plasmonic side polished FMF sensor with Au nanofilm for detection of prostate specific antigen with a sensitivity of 2500 nm/RIU. Recently, Dong et al. [6] investigated the performance of a plasmonic side polished few-mode fiber with Au, with the highest sensitivity of 4903 nm/RIU and a FOM of 46.1 RIU^{-1}. They successfully demonstrated the testing of bovine serum albumin (BSA) solution using the sensor.

While these reports highlight the potential of plasmonic fiber-optic sensors, there are three major issues associated with prior designs. The first problem is the complexity of some of the proposed structures (e.g., various hole dimensions, different materials) and the corresponding fabrication-induced imperfections. The second problem is the high cost of these devices for mass production as they usually utilize gold nanofilms. Finally, the sensitivity and FOM in these structures are typically not maximized as only noble metals (Au or Ag) have been studied as the main plasmonic material in past designs. Moreover, in most of these investigations, the effects of peak FWHM and FOM have not been addressed.

The most common plasmonic materials used in previously reported SPR sensors (based on optical fiber or prism designs) are Au and Ag because of their strong plasmonic response in the visible spectral region and their compatibility with biological samples [11]. However, their relatively high cost is a major drawback to the mass manufacturing of plasmonic devices containing them [11]. Furthermore, Ag is susceptible to surface oxidation in direct contact with air or water, while Au can soften at relatively low temperatures [11–13]. These limitations can significantly reduce the plasmonic efficiency of these noble metals [11]. An ideal alternative plasmonic material would offer lower production cost, higher melting point, higher chemical stability, and the possibility of chemical synthesis using available nano-fabrication methods [11–14]. Refractory materials, and in particular group IV transition metal nitrides (TMNs), have very high melting points and excellent chemical stabilities [11, 14]. TMNs also have a similar plasmonic response to Au and Ag in visible-near IR region [12]. While titanium nitride (TiN) has already received some attention as a promising candidate for plasmonic applications at visible and near-infrared regions [13, 14], other group IV TMNs, including zirconium nitride (ZrN) and hafnium nitride (HfN), remain unexplored. However, the few related previous studies have demonstrated the superior plasmonic performance of HfN compared to Au and even TiN for photothermal applications [15–17].

To address the challenges discussed above, herein, we used a numerical model to investigate simple miniaturized fiber-based SPR sensors by utilizing group IV nitrides and Au as the plasmonic materials in various geometries. We investigated two different plasmonic fiber-optic sensor designs based on simple single-mode fiber (SMF) and a few-mode fiber (FMF). The main reasons for choosing SMF and FMF are their simplicity and low cost which render the final

sensor easy to fabricate and cost efficient for mass production. We studied the sensor design, plasmonic materials, and the sensing mechanism. The role of design parameters on the resonance location was also investigated, and design parameters were optimized to achieve the highest sensitivity to variations in analyte RI. We also studied the spectral sensitivity, detection range, peak FWHM, and overall sensor FOM in the proposed fiber-optic sensors using various plasmonic materials.

Sensor Design

Fiber Design

In this section, we present a detailed description of the design of the proposed side-polished fiber-optic sensor. The schematic of a possible setup for a liquid sensing platform is demonstrated in Fig. 1a and consists of a broadband light source, a conventional fiber optic, and a side-polished sensing section [6]. The fabrication of side-polished, nanofilm-coated fibers has already been demonstrated, and there are several reported experimental studies on the possibilities of fabrication of such devices using wheel polishing techniques [3, 6]. After polishing one side of the fiber, the nanoparticles can be deposited on the polished fiber section to form a nanofilm. The deposition can be done using various techniques, for example, a vacuum evaporating method [6]. The liquid analyte will be in direct contact with the plasmonic nanofilm at the polished fiber section. By measuring the transmission or absorption spectra using a detector (spectrometer), one can detect the RI and thus sense the physical and chemical properties of the liquid analyte. The cross-section of the SMF and FMF designs used in this study are demonstrated in Fig. 1b, c, respectively. The major design parameters of SMF and FMF are core diameter (d), total fiber diameter, vertical distance between core and plasmonic nanofilm (D_v), and plasmonic film thickness (t) (Fig. 1). The sensor dimensions were optimized based on numerical investigations to achieve maximum coupling between core and plasmonic mode.

To reflect typical design parameters of conventional fibers and in the case of SMF, we set the diameter of the fiber core d and fiber cladding D to be 9.2 and 125 μm, respectively. For FMF, we set d and D to be 19 and 125 μm, respectively. To achieve the best sensing performances, we set the thickness of TMN/Au nanofilms to be 40 nm and the vertical distance between the fiber core and nanofilms to be 10 nm. The finite element method was used to calculate the effective index of fiber and plasmonic modes in the proposed fiber. The simulations were conducted in COMSOL Multiphysics software. Perfectly matched layers boundary conditions and an ultra-fine mesh size with a minimum element size of 1 nm and a maximum element size of 500 nm were applied to the considered configurations. Moreover, rigorous convergence tests were conducted for all results to minimize calculations errors. Finally, results were analyzed using MATLAB R2019b.

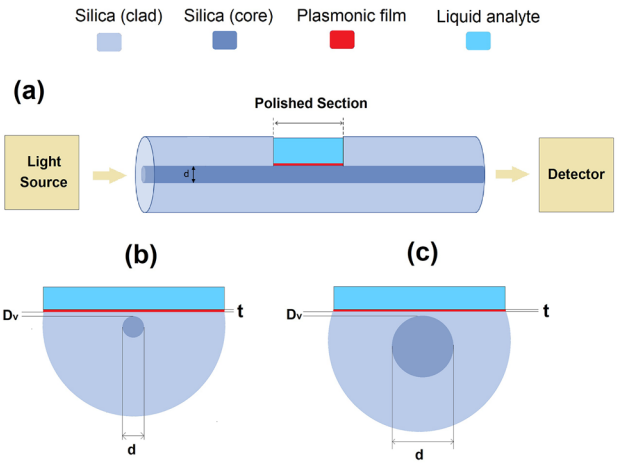

Fig. 1 **a** Schematic of a possible setup for liquid analyte detection using side-polished plasmonic fiber-optic sensors including a broadband light source at the fiber input and a detector (or spectrometer) at the fiber end. Cross-sectional view of the proposed **b** SMF and **c** FMF sensor. The design parameters of the SMF and FMF sensors are thickness of plasmonic film t, core diameter d, and vertical distance between core and film D_v

Materials and Modelling

To accurately simulate the material dispersion of silica (cladding material in the simulations), Sellmeier's equation [18] was utilized to determine the amount of silica RI for different excitation wavelengths:

$$n^2_{silica}(\lambda) = 1 + \frac{0.6961663\lambda^2}{\lambda^2 - 0.0684043^2} + \frac{0.4079426\lambda^2}{\lambda^2 - 0.1162414^2} + \frac{0.8974794\lambda^2}{\lambda^2 - 9.896161^2} \quad (1)$$

where λ is the excitation wavelength in μm. Note that in the SMF and FMF structures, the fiber core RI is chosen to be 0.36% higher than that of the cladding, similar to commercially available fibers [19]. To compare the plasmonic properties of different materials, one can use either complex RI or complex dielectric function as the two parameters are related [12]. The complex RI of Au was calculated using a Lorentz-Drude model obtained from a previous study [20], and the complex dielectric function of TMNs in our numerical analysis was obtained from the literature [12, 19]. We compared the real and imaginary components of dielectric function of TMNs and Au in Fig. 2. Figure 2a, b indicate that HfN and ZrN have smaller imaginary components (ε_2) and larger absolute real components (ε_1) in the visible range between 300 nm and 600 nm compared to Au.

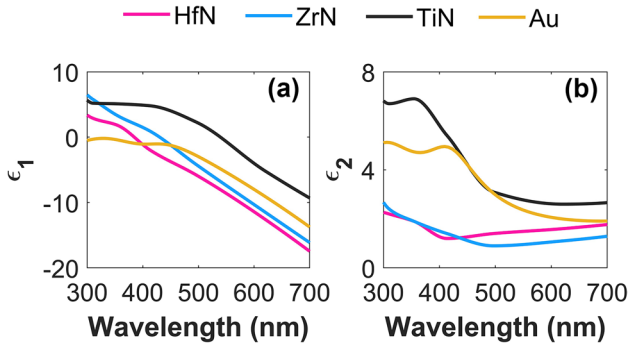

Fig. 2 **a** Real part and **b** imaginary part of dielectric function of HfN, ZrN, TiN, and Au in the visible range from 300 to 700 nm

The quality of a plasmonic material in SPs excitation can be quantified using the quality factor (Q_{factor}). In the case of surface plasmon polaritons which are electromagnetic waves excited on the surface of a nanofilm due to excitation of SPs, Q_{factor} can be defined as [21]

$$Q_{factor} = \frac{\varepsilon_1(\lambda)^2}{\varepsilon_2(\lambda)} \tag{2}$$

Figure 3 shows a comparison of the quality factors of TMNs and Au in the visible range. Based on our calculations, HfN and ZrN can markedly outperform Au in the visible range for applications related to surface plasmon polaritons excitation. In particular, the Q_{factor} of HfN is more than two times that of Au over the visible range. The smaller imaginary component of HfN and ZrN can also lead to a narrower peak, which is another important parameter in sensing applications. Narrower peaks are easier to detect by spectrometers, and therefore they will improve the sensor FOM. As such, one can expect to see better sensing performances

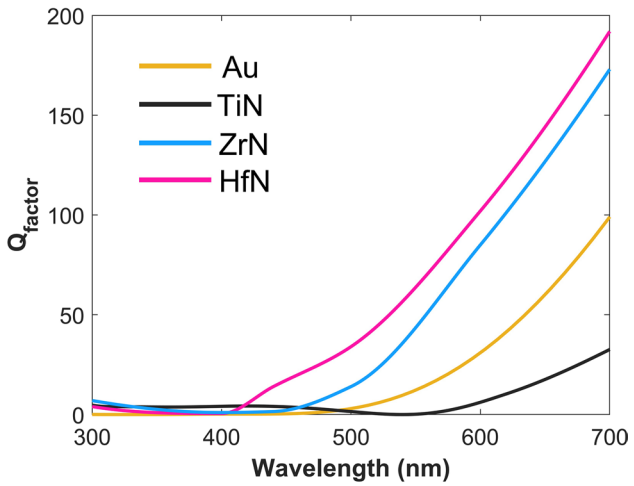

Fig. 3 Quality factor (Eq. 2) of TiN, ZrN and HfN compared to Au in the visible range from 300 to 700 nm

using HfN and ZrN comparing to Au. In the next sections, we test this hypothesis in the case of two different designs of plasmonic fiber-optic sensors.

Sensing Mechanism

To detect variations in a liquid analyte's RI, we monitor the variations in the loss maxima (or transmission dip) of light, while it propagates through the fiber (similar to Fig. 1a). A thin plasmonic nanofilm is introduced at the top of the polished fiber section to induce sensitivity to liquid RI (as seen in Fig. 1b, c). As we combine fiber optic and a plasmonic material, we can expect to see a merging of fiber and plasmonic modes in the resulting structure during excitation with a light source. When the effective mode index (n_{eff}) of the core mode ($n_{eff\text{-}core}$) matches with that of the nanofilm plasmonic mode ($n_{eff\text{-}film}$), the resonance condition is satisfied, resulting in maximum energy transfer from fiber mode to plasmonic mode and a power loss from fiber mode (or absorption from plasmonic mode) or a dip in fiber transmission spectra. The interaction between the plasmonic and fiber modes can lead to different amount of energy loss in various excitation wavelengths. We show that by changing the analyte RI, one can see different resonance frequencies and, consequently, detect an unknown liquid analyte based on the resonance location.

To make the sensing mechanism of the proposed plasmonic fiber-optic sensor clear, we plotted the variations of the effective index of the core mode $n_{eff\text{-}core}$, the effective index of the nanofilm plasmonic mode $n_{eff\text{-}film}$, and the imaginary component of the effective index of the core mode $Imag(n_{eff\text{-}core})$ as a function of wavelength for the SMF (Fig. 4a) and FMF (Fig. 4b) coated with HfN as the plasmonic material. The effective mode index of the fiber guided mode and the plasmonic mode of the HfN nanofilm intersect at a specific wavelength (resonance wavelength or λ_r) depending on the analyte RI. At resonance, maximum coupling between the two modes occurs, resulting in maximizing the imaginary component of the fiber mode effective index (Fig. 4). The imaginary component of the fiber mode is directly related to energy loss of the mode.

Therefore, a maximum in the imaginary component of the fiber mode effective index can result in forming a maximum in confinement loss (dip in transmission spectra) of the fiber. To monitor the variations of analyte RI, one can simply detect the loss maxima or the transmission dips of the sensor. Fiber confinement loss is directly proportional to the imaginary part of effective index of the fiber guiding mode [5, 6]:

$$a\ (dB/cm) = 8.686 \times 2\pi \times Im\left(n_{core}\right) \times 10^7/\lambda \tag{4}$$

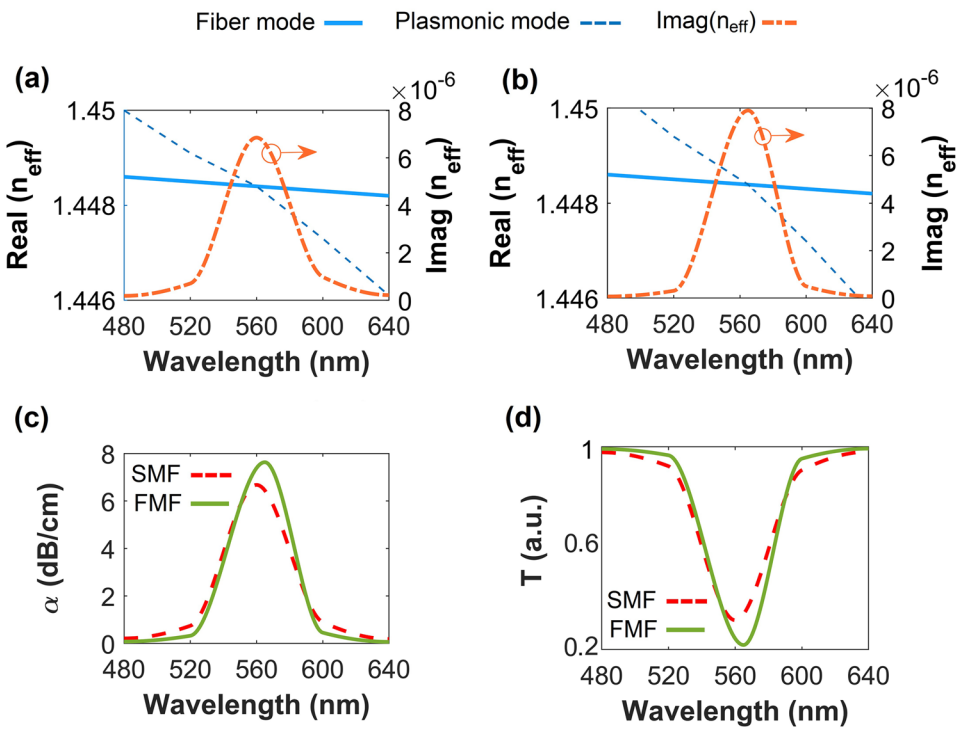

Fig. 4 Real (left *y*-axes) and imaginary (right *y*-axes) components of effective index (n_{eff}) of fiber modes (solid blue lines and dashed-dotted orange lines) and plasmonic modes (dashed blue lines) in **a** HfN-coated SMF and **b** HfN-coated FMF sensors. **c** Confinement loss spectra and **d** transmission spectra of the HfN-coated SMF and FMF sensors with analyte RI of 1.33. Design parameters t and D_v are set to be 40 and 10 nm, respectively

where λ is the operating wavelength in nm. The transmitted power *(T)* in the fiber is also proportional to the imaginary part of the effective index of the fiber mode. Transmission spectra can be obtained using Eq. 5 [6]:

$$\mathrm{T}(\lambda) = \exp\left[-\frac{4\pi}{\lambda} Im\left(n_{core}\right) \cdot \mathrm{L}\right] \tag{5}$$

where L is the fiber length in the polished section, which was herein considered to be 1 cm. Figure 4c, d show the confinement loss and transmission spectra of the corresponding guided modes in SMF and FMF. As expected, at resonance, one can see a loss maximum and a transmission dip.

To further analyze the interplay between fiber mode and HfN plasmonic mode, we studied the electric field distributions at the fiber core and surface of the plasmonic nanofilm. The electric field distributions of the corresponding fiber modes and coupled fiber-plasmonic modes at resonance in the proposed HfN-coated SMF and FMF are shown in Fig. 5 for reference. The fiber fundamental guided mode at λ = 480 nm (where there is no coupling between modes) and the coupled fiber/plasmonic mode of SMF at resonance (λ = 560 nm) are shown in Fig. 5a, b, respectively. Figure 5c presents a zoomed in view of the excited SPs on the surface of the HfN nanofilm.

FMF supports fundamental and higher order modes, including LP_{01} (Fig. 5d) and LP_{11} (Fig. 5g) modes. While both modes couple with plasmonic mode on the surface of the HfN nanofilm (Figs. 5e, h), the LP_{11a} mode of the FMF has stronger coupling and associated strong SP excitation, as clearly seen in Fig. 5i compared to Fig. 5f. Moreover, the penetration depth of the evanescent wave from the LP_{11} mode is larger than that of the LP_{01} mode. Strong coupling and the larger penetration depth of the coupled LP_{11} and plasmonic mode of HfN in FMF result in a relatively high sensitivity to variations in analyte RI. As a result, few mode fibers were more sensitive and more efficient in surface plasmon excitation and RI sensing than single mode fibers in this study. This is in agreement with previously reported FMF results [6]. As seen in Figs. 4 and 5, at resonance, the fiber mode loses a large portion of its energy to excite SPs, which result in transmission dip (or confinement loss maximum) in which the location and magnitude of the resonance strongly depends on the analyte RI. For SMF, the resonance wavelength is 560 nm, while the resonance wavelength for FMF is 564 nm in the case of an analyte RI of 1.33.

Before investigating the sensors performance, we analyze the role of selected design parameters on the location of resonance in the proposed FMF sensor with HfN as the plasmonic nanofilm material. We only considered FMF for studying the role of design parameters, as few-mode fibers can offer better sensitivity and stronger resonances compared to SMF. The variations of resonance wavelength depending on the design parameter for other materials (or for the SMF) follow the same trends. Here, we fixed the other design parameters, such as core diameter, and varied the plasmonic film thickness (Fig. 6a) or vertical distance between film and fiber (Fig. 6b). For these studies, we only considered HfN

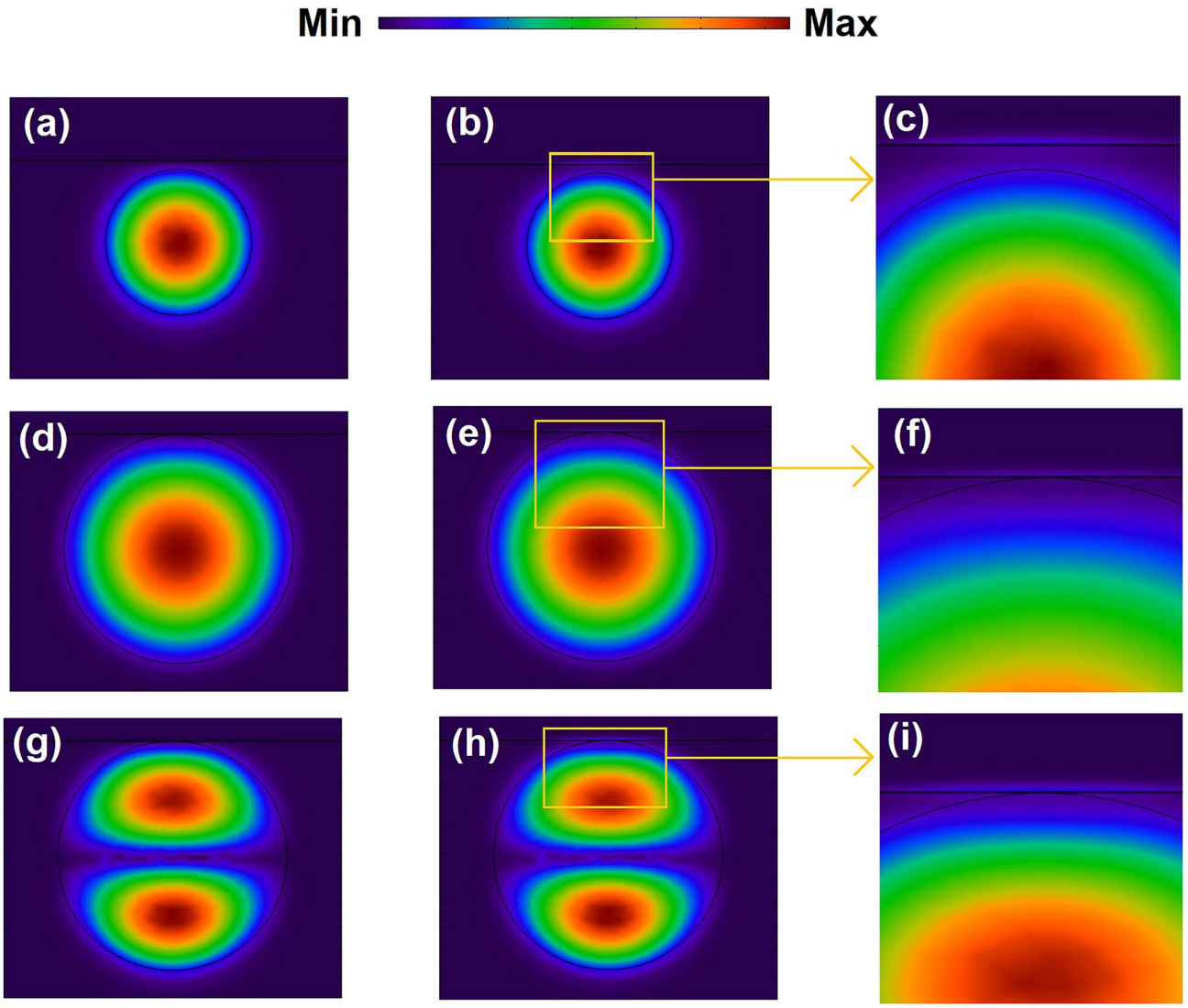

Fig. 5 Electric field distributions at the fiber core and surface of HfN nanofilm for **a–c** SMF with fundamental fiber mode, **d–f** FMF LP_{01} mode, and **g–i** FMF LP_{11a} mode. Note that (**a**), (**d**), and (**g**) are fiber modes off-resonance; (**b**), (**e**), and (**h**) demonstrate the coupled mode at resonance; and (**c**), (**f**), and (**i**) are zoomed-in views of surface plasmons on the HfN nanofilm for the coupled mode

as the plasmonic material and set the analyte RI to be 1.33, which is close to water RI at room temperature.

Increasing the thickness of the plasmonic film from 20 to 60 nm produced loss maximum (or λ_r) redshifts from 495 to 597 nm (Fig. 6a). Also, the confinement loss magnitude was greatly reduced by increasing the HfN nanofilm thickness. Additionally, when $t = 40$ nm, the loss peak is narrowest with a peak FWHM of 36 nm. Next, we studied the role of vertical distance between fiber core and plasmonic film on the resonance location. By increasing the D_v from 10 to 30 nm, λ_r slightly blueshifts from 561 to 557 nm with a decrease in the magnitude (Fig. 6b). The peak FWHM increased with an increasing D_v. In addition to resonance location, magnitude, and FWHM, changing D_v or t can also influence the sensor sensitivity and peak FWHM. Our extensive numerical simulations reveal that to obtain maximum sensitivity in FMF for liquid analytes in the range of 1.33 and 1.38, one should set the D_v and t to be 10 and 40 nm, respectively. Additionally, the optimized design parameters lead to the narrowest FWHM and strong confinement loss due to strong coupling between core and plasmonic modes (Fig. 5). In the next section, we use the optimized design parameters and analyze the sensing performance of our proposed SMF and FMF sensors with various materials, including TMNs and Au.

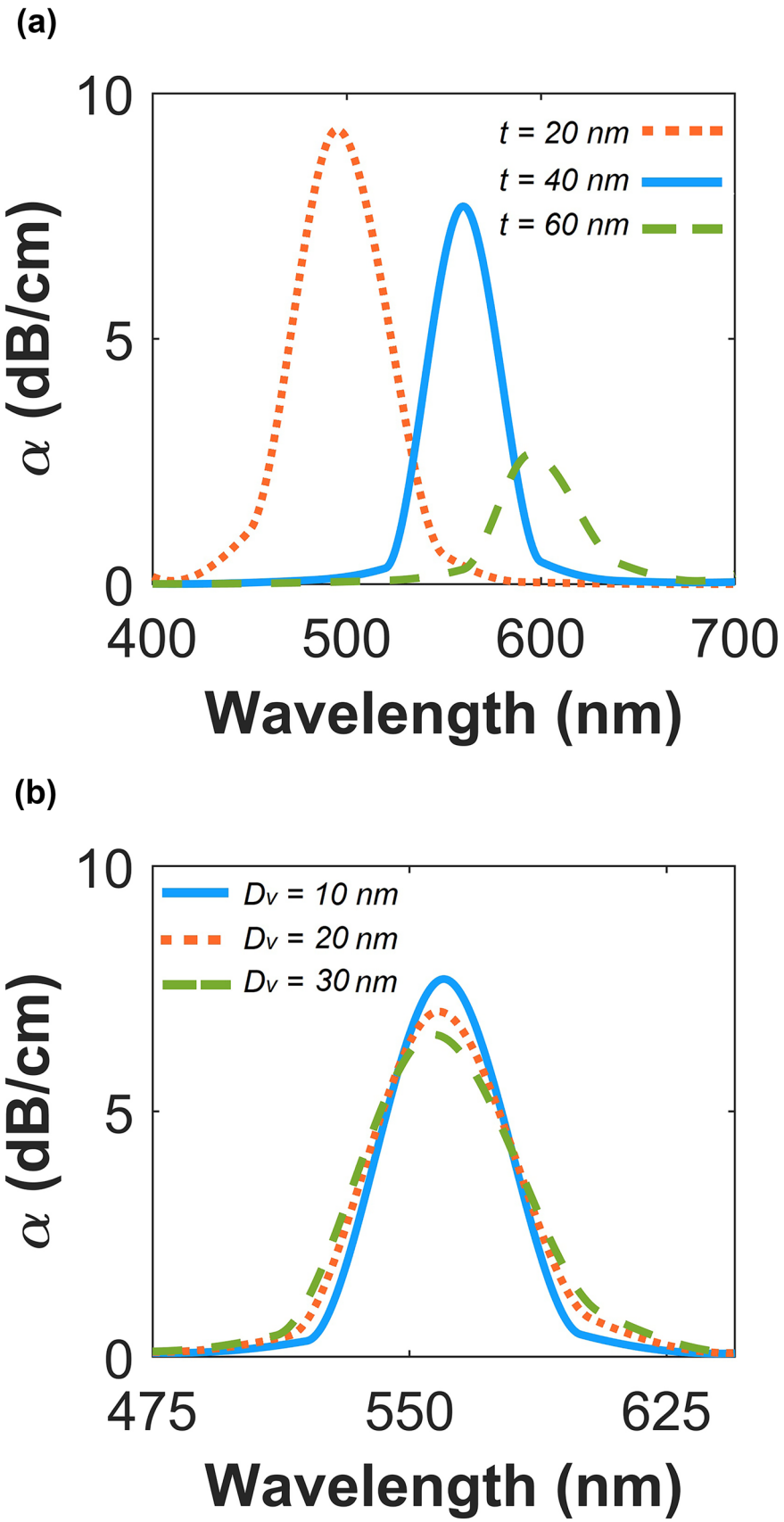

Fig. 6 The role of design parameters on the confinement loss spectra and resonance location of HfN-coated FMF sensors: **a** the role of thickness of HfN nanofilm and **b** the role of vertical distance between the core and HfN nanofilm

Sensing Performances

In this section, the sensing performances including the spectral sensitivity, peak FWHM, and FOM of the proposed SMF and FMF sensors are studied in detail. The variations of resonance wavelength for the proposed SMF and FMF sensors, with Au, TiN, ZrN, and HfN as the plasmonic material, and with optimized design parameters as a function of analyte RI are shown in Fig. 7a, b, respectively. While TiN performed similarly to Au, HfN and ZrN outperform Au with more than three times larger sensitivity to variations in analyte RI. It is also important to note that FMF offers higher sensitivities than SMF, particularly due to the strong mode coupling between LP_{11} fiber mode and plasmonic mode. Particularly for the FMF coated with HfN (Fig. 7b), the resonance wavelength shifts from 564 to 871 nm (307 nm shift) by increasing the analyte RI from 1.33 to 1.38, which is more than three times larger than the 86 nm shift for FMF coated with Au. While both HfN and ZrN demonstrate excellent sensitivity to variations in analyte RI, HfN outperforms ZrN with a slightly higher sensitivity. The spectral sensitivity of a fiber-optic sensor can be calculated as follows [5, 6]:

$$\mathrm{S\ (nm/RIU)} = \frac{\Delta\lambda_r}{\Delta n_{analyte}} \tag{6}$$

where $\Delta\lambda_r$ is the shift in resonance wavelength depending on the change in analyte refractive index ($\Delta n_{analyte}$).

The average spectral sensitivity in the case of FMF coated with HfN for analyte RI between 1.33 and 1.38 was 6140 nm/RIU (Fig. 8c), with a maximum spectral sensitivity of 8200 nm/RIU around 1.34 (Fig. 8d). This sensitivity is more than three times larger than that of the FMF coated with Au nanofilm. According to the simulated results, the sensor resonance redshifts and broadens with increasing analyte RI. For analyte RIs larger than 1.38, the broadness of the resonance makes it difficult to detect the peaks and reduces sensor sensitivity. While the sensor can detect analyte RIs smaller than 1.33, the relationship between resonance wavelength and RI is not linear for smaller RIs. These facts limit

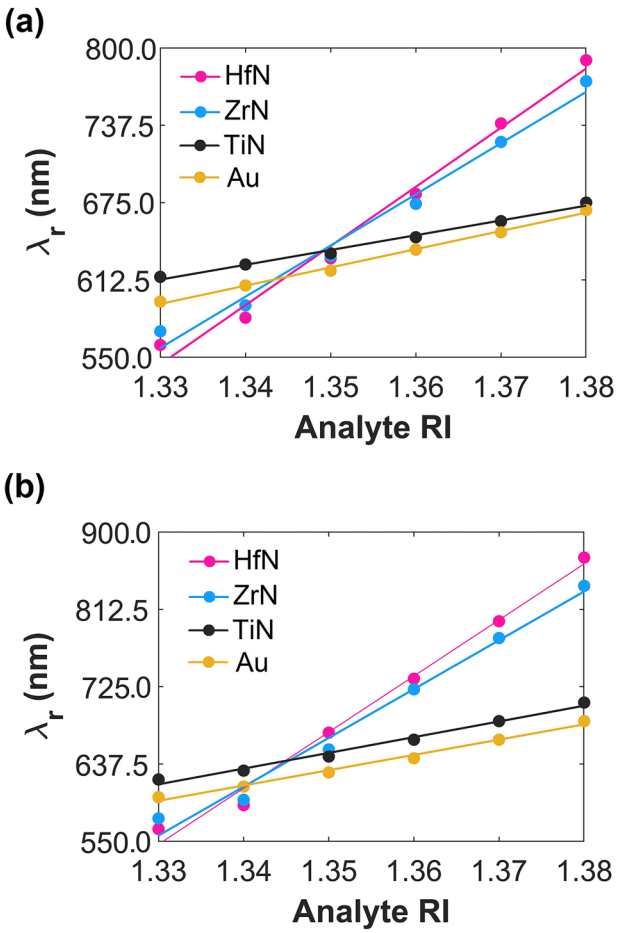

Fig. 7 Variations of resonance wavelength depending on analyte RI for **a** SMF and **b** FMF sensors with various plasmonic materials

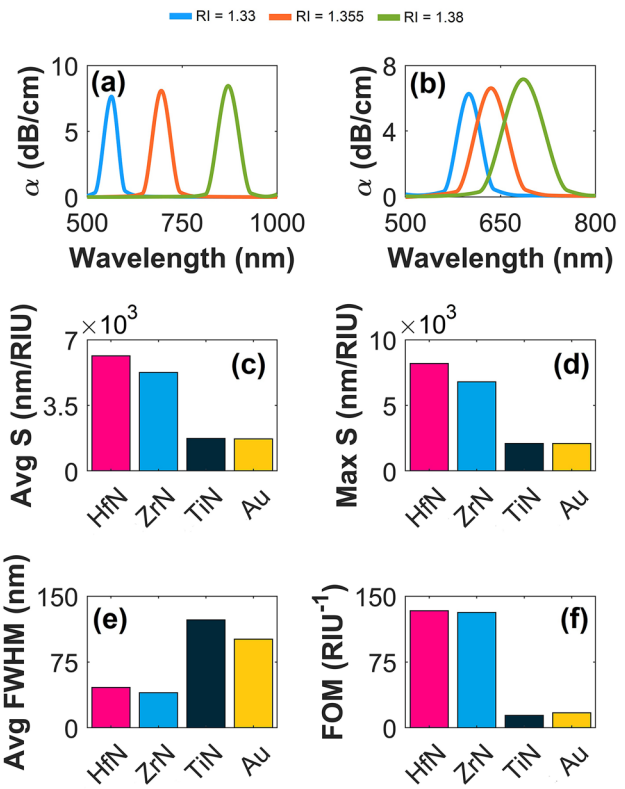

Fig. 8 Confinement loss spectra of FMF sensor coated with **a** HfN and **b** Au for different analyte RIs ranging from 1.33 to 1.38. Comparison between various plasmonic materials in FMF sensors using different sensing performance parameters: **c** average linear sensitivity, **d** maximum sensitivity, **e** average peak FWHM, and **f** average overall sensor figure of merit

Table 1 Comparison between sensing performances of the proposed HfN-coated FMF sensor and similar fiber-optic sensors in the literature

Plasmonic material	Detection range	Max sensitivity (nm/RIU)	Max FOM (RIU^{-1})
HfN (This work)	1.33–1.38	8200	201
Au - Ref. [6]	1.33–1.404	4903	46.1
Au - Ref. [22]	1.33–1.391	2278	Not reported
Graphene and Ag - Ref. [9]	1.33–1.36	3700	Not reported

the linear detection range of our sensor to 0.05 refractive index unit (RIU) from 1.33 to 1.38. Note that the variations in resonance wavelength of the FMF coated with HfN are linear with a change in analyte RI between 1.33 and 1.38 and the coefficient of determination for linear fit is 0.984.

For reference, we also plotted the loss spectra of the FMF coated with HfN and Au, while varying analyte RI from 1.33 (Fig. 8a) to 1.38 (Fig. 8b).

HfN not only offers better sensitivities but also narrower peaks (smaller peak FWHM), which can allow easier detection of analytes. The overall performance of a fiber-optic sensor can be evaluated using FOM, which is usually defined as the ratio between sensitivity and peak FWHM for spectral-based SPR sensors [6]:

$$\mathrm{FOM}\left(\mathrm{RIU}^{-1}\right) = \frac{S(\frac{nm}{RIU})}{FWHM(nm)} \tag{7}$$

We compared the average sensitivity, maximum sensitivity, average peak FWHM, and average FOM of the proposed FMF using various plasmonic nanofilms (HfN, ZrN, TiN, Au) in Fig. 8c–f. Evidently, coating the fiber with HfN and ZrN would significantly improve the sensing performance of the fiber-optic sensors (particularly FMF) compared to coating the fiber with Au or TiN. Compared to ZrN, HfN offers better average and maximum sensitivities (6140 for 1.33–1.38 and 8200 nm/RIU around 1.34 for HfN, compared to 5260 for 1.33–138 and 6800 nm/RIU around 1.34 for ZrN). Among the various coating materials considered, FMF coated with ZrN has the lowest average peak FWHM of 40 nm followed by HfN with an average peak FWHM of 46 nm (Fig. 8e). However, the data in Fig. 8f suggest that the average overall FOM of HfN-coated FMF (133.5) is similar to that for FMF coated with ZrN (131.5). Furthermore, the average FOM of the HfN-coated FMF (133.5) is almost eight times larger than that of Au-coated FMF (17). These results highlight the possible applications of group IV TMNs, especially HfN, in sensing applications based on plasmonic fiber-optic sensors as alternative and better materials compared to Au.

Finally, we compared the sensing performance of our proposed HfN-coated FMF with previously reported fiber-optic sensor performance. Note that for this comparison, we only considered the previously reported simple side polished SMFs and FMFs (and one example of simple photonic crystal fibers) and excluded any complex structure (like photonic crystal fibers with various air hole diameters). As seen in Table 1, our proposed HfN-coated FMF offer better sensitivities and significantly better FOM compared to previously reported similar sensors. While the average FOM of HfN-coated FMF is 133, the maximum FOM of HfN-coated FMF can be as large as 201 around an analyte RI of 1.34, which is more than four times that for previously reported fiber-optic sensors [6]. Another important advantage of the proposed fiber-optic sensors coated with TMNs are linear sensitivity across the whole analyte RI range, compared to previously reported studies that do not offer linear sensitivities for the whole range of analyte RIs.

Conclusions

In conclusion, we designed simple single mode and few mode side-polished plasmonic fiber-optic sensors using group IV transition metal nitrides including HfN, ZrN and TiN nanofilms. We compared the sensing performances of the proposed sensors including average sensitivity, maximum sensitivity, and average full width at half maximum and figure of merit, with similar Au-based plasmonic fiber-optic sensors. The results suggest that HfN and ZrN can considerably outperform Au in the visible region as alternative plasmonic materials for the design of fiber-optic sensors with more than three times larger sensitivity and a sensing figure of merit of almost eight times that of Au. In particular, a simple HfN-coated few-mode optical fiber sensor can demonstrate an average linear sensitivity of 6140 nm/RIU and an average figure of merit of 133 for analyte refractive indices between 1.33 and 1.38. The results presented in here can be transformative for design and development of plasmonic fiber-optic sensors in different fields including environmental sensing, biology, and medicine, as it allows us to develop and deploy simple and cost-effective sensors with large sensitivities for monitoring various physical and chemical properties of liquid analytes.

Author Contribution The manuscript was written through contributions of all authors.

Funding This research was supported by the Ocean Frontier Institute through an award from the Canada First Research Excellence Fund. CMC Microsystems Canada and Dalhousie University are thanked for providing the access to COMSOL Multiphysics, and MATLAB.

Availability of Data and Material All data generated or analyzed during this study are included in this published article.

Declarations

Ethics Approval Not applicable.

Consent to Participate Not applicable.

Consent for Publication All authors read and approved the final manuscript for publication.

Conflict of Interest The authors declare no competing interests.

References

1. Stockman MI (2011) Nanoplasmonics: past, present, and glimpse into future. Opt Express 19:22029–22106
2. Luan N, Yao J (2017) Refractive index and temperature sensing based on surface plasmon resonance and directional resonance coupling in a PCF. IEEE Photon J 9:2
3. Monfared YE (2020) Overview of recent advances in the design of plasmonic fiber-optic biosensors. Biosensors 10:77
4. Si Y, Lao J, Zhang X, Liu Y, Cai S, Vila A, Li K, Huang Y, Yuan Y, Caucheteur C, Guo T (2019) Electrochemical plasmonic fiber-optic sensors for ultra-sensitive heavy metal detection. J Lightwave Technol 37(14):3495–3502
5. Monfared YE, Hajati M, Liang C, Yang S, Qasymeh M (2021) Quasi-D-shaped fiber optic plasmonic biosensor for high-index analyte detection. IEEE Sensors 21:17–23
6. Dong J, Zhang Y, Wang Y, Yang F, Hu S, Chen Y, Zhu W, Qiu W, Guan H, Lu H, Yu J, Zhong Y, Zhang J, Luo Y, Chen Z (2018) Side-polished few-mode fiber based surface plasmon resonance biosensor. Opt Express 27(8):11348
7. Coelho L, De Almeida J, Santos JL, Ferreira RAS, André PS, Viegas D (2015) Sensing structure based on surface plasmon resonance in chemically etched single mode optical fibres. Plasmonics 10(2):319–327
8. Mao P, Luo Y, Chen C, Peng S, Feng X, Tang J, Fang J, Zhang J, Lu H, Yu J, Chen Z (2015) Design and optimization of surface plasmon resonance sensor based on multimode fiber. Opt Quantum Electron 47(6):1495–1502
9. Dash JJ, Jha R (2015) On the performance of graphene-based D-shaped photonic crystal fibre biosensor using surface plasmon resonance. Plasmonics 10(5):1123–1131
10. Jang HS, Park KN, Kang CD, Kim JP, Sim SJ, Lee KS (2009) Optical fiber SPR biosensor with sandwich assay for the detection of prostate specific antigen. Opt Commun 282(14):2827–2830
11. Karaballi RA, Monfared YE, Dasog M (2020) Overview of synthetic methods to prepare plasmonic transition metal nitride nanoparticles. Chemistry A European Journal 26:8499
12. Monfared YE, Dasog M (2021) Computational investigation of the plasmonic properties of TiN, ZrN, and HfN nanoparticles: The role of particle size, medium, and surface oxidation. Can J Chem 99(7):576–584
13. Rodriguez C, Barragan A, Nava G, Exarhos S, Mangolini L (2020) Stabilizing the plasmonic response of titanium nitride nanocrystals with a silicon oxynitride shell: implications for refractory optical materials. ACS Appl Nano Mater 3(5):4504–4511
14. Naik GV, Schroeder JL, Ni X, Kildishev AV, Sands TD, Boltasseva A (2012) Titanium nitride as a plasmonic material for visible and near-infrared wavelengths. Opt Mater Express 2:478–489
15. Margeson MJ, Dasog M (2020) Plasmonic metal nitrides for solar-driven water evaporation. Environ Sci: Water Res Technol 6:3169–3177
16. Traver E, Karaballi RA, Monfared YE, Daurie H, Gagnon GA, Dasog M (2020) TiN, ZrN, and HfN nanoparticles on nanoporous aluminum oxide membranes for solar-driven water evaporation and desalination. ACS Appl Nano Mater 3:2787–2794
17. Karaballi RA, Monfared YE, Dasog M (2020) Photothermal transduction efficiencies of plasmonic Group 4 metal nitride nanocrystals. Langmuir 36(18):5058–5064
18. Tan Z (1998) Determination of refractive index of silica glass for infrared wavelengths by IR spectroscopy. J Non-Cryst Solids 223:158–163
19. Cusano A, Iadicicco A, Pilla P, Contessa L, Campopiano S, Cutolo A, Giordano M (2006) Mode transition in high refractive index coated long period gratings. Opt Express 14:19–34
20. Rakić D, Djurišic AB, Elazar JM, Majewski ML (1998) Optical properties of metallic films for vertical-cavity optoelectronic devices. Appl Opt 37:5271–5283
21. Kumar M, Umezawa N, Ishii S, Nagao T (2016) Examining the performance of refractory conductive ceramics as plasmonic materials: A theoretical approach. ACS Photonics 3:43–50
22. Ding ZW, Lang TT, Wang Y, Zhao CL (2017) Surface plasmon resonance refractive index sensor based on tapered coreless optical fiber structure. J Lightwave Technol 35(21):4734–4739

Publisher's Note Springer Nature remains neutral with regard to jurisdictional claims in published maps and institutional affiliations.